

Simulation of an Interferometric Fiber Optic Gyroscope Applied to a Rocket Model

Gabriel F. S. Nunes^{1,2}, Antônio P. S. D. Carvalho¹, Adalberto J. A. Tavares Júnior¹, Luis G. R. Vito¹,
João M. S. Sakamoto^{2,1} and Neusa M. F. Oliveira¹

¹Aeronautics Institute of Technology (ITA), Praça Mal. Eduardo Gomes, 50, São José dos Campos, SP 12228-900, Brazil

²Institute for Advanced Studies (IEAv), Trevo Cel. Av. José A. A. do Amarante, 1, São José dos Campos, SP 12228-001, Brazil

Abstract—In this work, a navigation and control algorithm of a microsatellite launch vehicle was simulated together with noise models representing real gyroscopes. Three gyroscope noise models were studied and validated by calculating the Allan variance. Then, the trajectory was simulated to compare two types of gyroscope, one interferometric optic fiber gyroscope and one micro-electro-mechanical system gyroscope. The difference between the reference trajectory and the trajectory calculated using an ideal gyroscope is 0.20 km ($\approx 1\%$ error). The difference between the reference trajectory and the trajectory with the IFOG is 4.66 km ($\approx 16\%$ error). The difference between the reference trajectory and the trajectory with the MEMS is 5.92 km ($\approx 20\%$ error). As for the final attitude, it showed a negligible error with both types of gyroscopes. The results showed that the navigation and control algorithm used was able to correctly stabilize the vehicle's attitude. However, it still requires improvements to follow the desired trajectory and not just the attitude.

Keywords—Gyroscope, rockets, sensor noise, optical fiber, simulation.

I. INTRODUCTION

There are only a few countries with the technology and know-how to launch satellites [1]. On the other hand, in the last decade there was a rapid rise in the number of on-orbit objects. Therefore, this demand due to the current space race (e.g., communication satellite constellations) highlights the importance of the development of technology necessary to launch satellites, microsatellites, and nanosatellites [2].

The technology to control and navigate a microsatellite launch vehicle (MLV) is similar to the needed for other purposes rockets, for example, those for military applications [3]. One fundamental component needed to navigate a rocket is an inertial measurement unit (IMU). An IMU is a collection of inertial sensors resulting in measurements of two or more degrees of freedom, typically it is encapsulated in just one device to provide six degrees of freedom. In this case, it is composed of three accelerometers, three gyroscopes, and it may include a magnetometer (even though the magnetometer is not an inertial sensor) [3].

For simple applications involving short trips and available communication with external navigation sensors, it is commonly used IMU made of micro-electro-mechanical systems (MEMS). However, as the strategic relevance of the application increases it also increases the need for a more reliable and sensitive IMU. Navigation with low-grade IMUs

usually requires some kind of sensor fusion, e.g., with global positioning system (GPS). Being able to navigate a vehicle without external sensors is a strategic action taken to avoid potential vulnerabilities [4].

Interferometric fiber optic gyroscopes (IFOG) are important devices in the field of inertial sensors and are considered an alternative technology to the mechanical method and ring laser gyroscopes, for inertial navigation and control applications [5]. IFOG are considered an all-important sensor for precision inertial navigation systems, due to their low cost in comparison to a ring laser gyroscope, small size, low power consumption, and high reliability [6], [7]. Due to its advantages, studies are being carried out to evaluate the application of IFOG, from the simplest to the most complex and challenging environments and vehicles, such as missile launch vehicles, satellite launch vehicles, rockets, and other types of vehicles.

A. Problem Statement

In this work, a model of an IFOG is included in the general diagram of the control and navigation system of an MLV, Fig. 1. Previously, the navigation and control system considered an ideal estimation of the angular velocities, that is, the angular velocities were measured by ideal gyroscopes without any noise and offset [1]. In this work, the simulation takes into account a realistic measurement signal provided by a simulation of an IFOG that was modeled using a Brazilian IFOG as a reference [8]. Also, a MEMS gyroscope is included in the MLV simulation to be used as a comparison.

Considering a realistic estimation of the angular velocities increases the meaningfulness of the simulation. The vehicle representing the microsatellite launch vehicle is the Brazilian VLM-1 rocket. The simulation trajectory is the first launch stage with a duration of 83 s and the launch starts in the *Centro de Lançamento de Alcântara*, in Maranhão, Brazil [10].

The objective is to compare the simulated MLV trajectory using ideal gyroscopes, using simulated IFOGs representing Brazil's technology, and using a commercially available tactical grade MEMS gyroscope.

II. GYROSCOPE NOISES

Gyroscopes are inertial sensors that measure angular velocity, commonly represented in degrees per second ($^{\circ}/s$). They can be constructed based on different technologies, for example, mechanical gyroscopes, vibratory gyroscopes, MEMS gyroscopes, ring laser gyroscopes, and fiber optic gyroscopes [11].

G.F.S. Nunes, nunesgfs@gmail.com; A.P.S.D. Carvalho, engantonio@poli.ufrj.br; A.J.A. Tavares Júnior, adalbertotjr@yahoo.com.br; L.G.R. Vito, gustavoaru@hotmail.com; J.M.S. Sakamoto, sakamotojmss@fab.mil.br; N.M.F. Oliveira, neusa@ita.br.

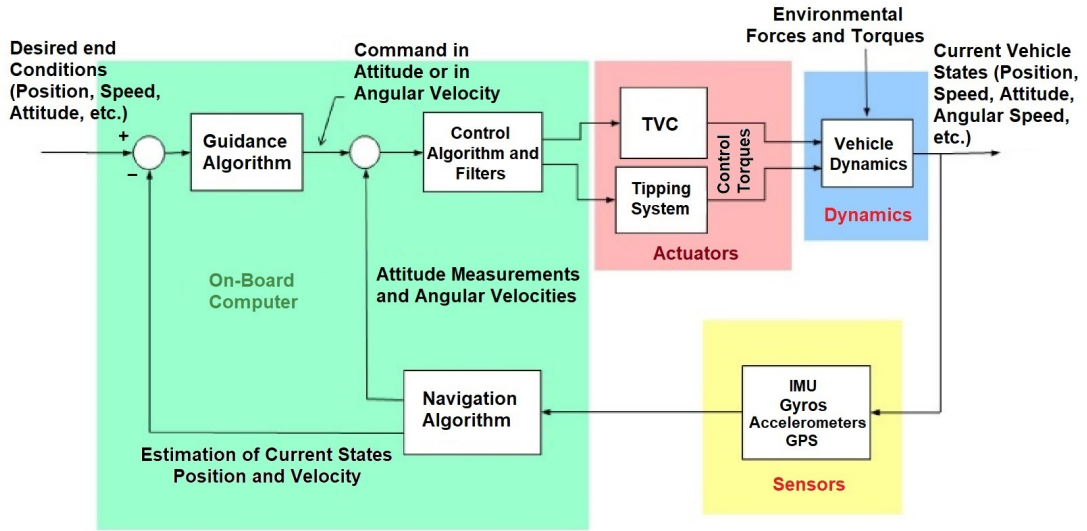


Fig. 1. Block diagram of a satellite launch vehicle [9].

IFOG are very sensitive sensors that can even measure a fraction of Earth's angular velocity. The difference among the types of gyroscopes can be represented in terms of their sensitivities, dynamic range, instability (drift), and noise level. Usually, the characterization of a gyroscope is represented by an Allan variance which provides the angle random walk (ARW) and the bias drift [8], [12].

The IFOG simulated in this work uses the noise values presented by [8].

The angle random walk is the white noise of the gyroscopes and is usually provided in units of $^{\circ}/\sqrt{h}$. It can be interpreted as follows, after x hours the standard deviation of the integrated angular velocity, the angle, is the ARW value multiplied by \sqrt{x} [13].

To convert the ARW to units of power spectral density (1) is used

$$1 \left[^{\circ}/\sqrt{h} \right] = 60 \left[^{\circ}/h/\sqrt{Hz} \right]. \quad (1)$$

To simulate the white noise it is needed a value of variance, or standard deviation, to feed a random number generator algorithm. The standard deviation can be calculated by [13]:

$$\sigma \left[^{\circ}/h \right] = ARW \left[^{\circ}/\sqrt{h} \right] \cdot 60 \cdot \sqrt{\Delta f [Hz]}. \quad (2)$$

It can be seen that the integration of the spectral density over the bandwidth of the sensor is equivalent to its root mean square value (RMS). Thus, since the mean value of noise is zero, the RMS value is the standard deviation represented in (2).

A simple preliminary simulation, as shown in Fig. 2, was performed to show the effect in the recovered angle due to the ARW noise. Two values of ARW were used, one representing a commercial MEMS gyroscope present in the inertial measurement unit (IMU) model STIM300 with ARW of $0.15 \text{ } ^{\circ}/\sqrt{h}$ [14] and the other representing the reference IFOG chosen in this work with ARW of $5.4 \cdot 10^{-4} \text{ } ^{\circ}/\sqrt{h}$ [8]. One thousand simulations were carried out with $0 \text{ } ^{\circ}/s$ input for each ARW value, considering the same bandwidth of 5 Hz and using (2) to generate a Gaussian distribution.

The output angle value over time is shown in Fig. 3 for one thousand simulations. The blue lines are the simulations

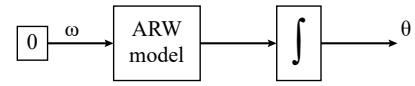


Fig. 2. Block diagram to check the effect of different ARW values in the final estimated angular position.

representing the IFOG and the black lines represent the MEMS gyroscope. It is possible to see that the simulations for both sensors have the same behavior over time, but the angle error due to the IFOG ARW value is substantially lower in comparison with the MEMS error.

The histograms in Fig. 4 show the final angles after 1 h of navigation for each sensor in Fig. 3. The standard deviation in Fig. 4a is approximately the ARW value of the MEMS gyroscope and the standard deviation of Fig. 4b is approximately the ARW of the IFOG. Therefore, agreeing with the interpretation of the ARW presented in units of $^{\circ}/\sqrt{h}$.

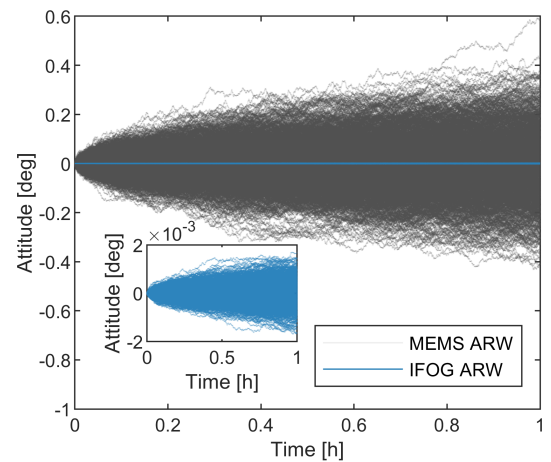


Fig. 3. Error in attitude due to angle random walk.

Another parameter is the bias instability which is a slow variation of the bias value and is presented in units of the measurement itself, $^{\circ}/h$. This noise is attributed to the electronics in the sensor and other components with random

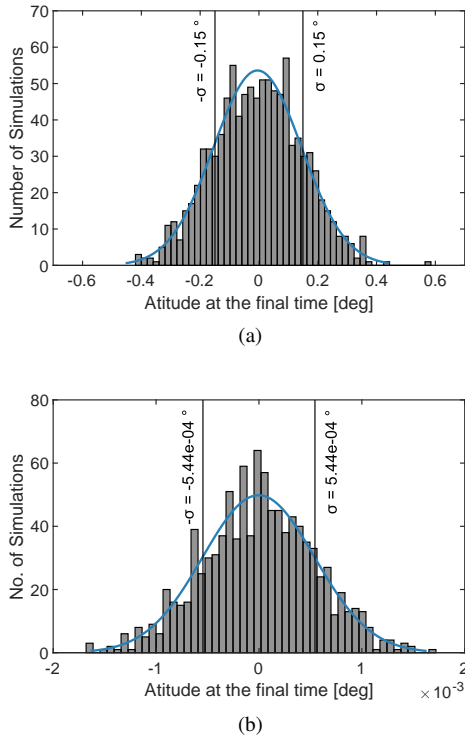


Fig. 4. Histogram of position after 1 hour for 1000 simulations for the gyroscope (a) STIM300 and (b) IFOG.

flickering. It is also called flickering noise or $1/f$ noise [15].

Two sensors can have the same order of magnitude of bias instability, but different stability times. This can be checked from an Allan deviation plot (explained in more detail in Section III). The minimum value of the Allan deviation is proportional to the bias instability value, but the longer it takes to reach the minimum, the longer the sensor is stable with the given instability value [16].

Another noise is the rate random walk (RRW), which has not yet been a consensus on its origin. It is a very long time-correlated noise, which can be viewed as the measurement acceleration, or in this case, the angular acceleration [15]. Additionally, RRW noise value is usually not provided by authors in publications about inertial sensors, nor in data sheets of commercial sensors. Despite this fact, it has recently been proved the essential importance of the RRW noise for longer duration flights [17]. So, in this work, the RRW noise was estimated when not provided.

III. METHODOLOGY

To simulate an IFOG signal there are a few options, one of them is to use the noise models provided by the very detailed study by Jerath, Brennan, and Lagoa [15], called here as model 1. In this model, the bias instability is simulated as a truncated infinite impulse response (IIR) filter over a white noise signal [15]. The ARW is simulated as a random Gaussian distribution with standard deviation calculated using an equation equivalent to (2), taking into consideration the sensor bandwidth. The RRW is simulated similarly to the ARW, with a random Gaussian distribution integrated over the sampling frequency.

Alternatively, there is a Matlab function called *imuSensor* introduced in version R2019b included in the navigation

toolbox, called here as model 2. This simulates the noise for an entire inertial measurement unit, including gyroscopes, accelerometers, and magnetometers. To simulate just the gyroscope, the other sensors are fed with arrays of zeros in the input, and just the output of the gyroscope is considered.

Finally, model 3 is based on [18], which simulates the ARW as random variation and RRW as random variation integrated in time. The bias instability is simulated as a simple random variation representing the change of polarization in the optical fiber, or by using a more complex model to represent the $1/f$ noise. The simulation can be achieved by using (2) to calculate the standard deviation to feed the random Gaussian number generator algorithm representing the ARW noise. The bias instability can be simulated by the noise value as the standard deviation of a random Gaussian distribution which is then integrated. The integration method is a good choice to emulate the bias instability and generate a signal response with characteristics of a signal containing RRW at the same time. Because the integrator works as a low-pass filter, it is similar to model 1 which uses the IIR filter. Also compared to model 1, the RRW is an integration of the white noise. Model 3 was assembled using Simulink, as shown in Fig. 5.

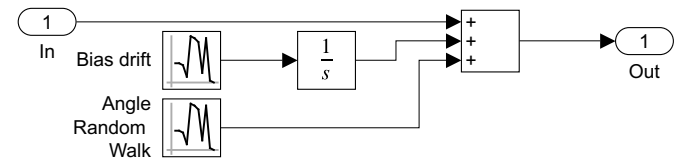


Fig. 5. Simulink block diagram for model 3.

All three models were simulated using the values of ARW ($5.40 \cdot 10^{-4} \text{ }^\circ/\sqrt{\text{h}}$) and bias instability ($1.70 \cdot 10^{-3} \text{ }^\circ/\text{h}$) from [8], and a guessed value for RRW ($4.32 \cdot 10^{-2} \text{ }^\circ/\text{h}/\sqrt{\text{h}}$) that resulted in comparable Allan deviation plots to the Allan deviation plot showed by [8].

To validate the simulated signals, the noises were recovered using an Allan variance calculation. Allan variance is a common method used to characterize inertial sensors, accelerometers and gyroscopes [8], [12], [15], [19]. It is a time-domain characterization of multiple types of noise and can be related to the power spectral density.

The conditions needed to calculate the Allan variance are to acquire the sensor signal without an input signal disturbing the measurements, at a constant temperature, and constant acquisition sample period. Inertial sensors usually present a signal in the input, the gravity acceleration for the accelerometers and the Earth's rotation for gyroscopes. However, these signals have no impact on the characterization because they are fairly constant signals.

A long-duration signal is necessary to measure the slowly correlated noises, for example, the bias instability and RRW. This calculation can demand a lot of time and be computationally expensive. Studies aiming to solve this problem can be found in the literature [20], [21], [22].

A signal with 10 h duration, an input of $0 \text{ }^\circ/\text{h}$, and a sample rate of 100 Hz was simulated using Models 1, 2, and 3, resulting in three simulated output signals. Then, the fully overlapped Allan variance was calculated according to the IEEE standard 952-2020 [23]. After the Allan variance is calculated, a plot of its square root (Allan deviation) can

be used to recover the noise values from it. A visual analysis was performed in the Allan deviation plot (in seconds by $^{\circ}/h$), in log-log scale, to recover the noise values of the simulated output signals [15]. A very helpful table, with conversions to recover noise values from the Allan deviation plot for gyroscopes and accelerometers, is presented in [20].

The ARW, in $^{\circ}/h/\sqrt{Hz}$, can be recovered from the equivalent Allan deviation value at the 1 s Allan time, and then applying the conversion in (1) to obtain the value in $^{\circ}/\sqrt{h}$. It is expected that the slope of the Allan deviation plot at the point 1 s is equal to $-1/2$ if there is only white noise in the sensor [23].

The minimum value of the Allan deviation, representing a zero slope, is used to obtain the bias instability. The bias instability in $^{\circ}/h$ is this minimum value divided by 0.664.

The RRW, in $^{\circ}/h/\sqrt{h}$, can be recovered by the point corresponding to the Allan time equal to 3 s for a line fitting the Allan deviation with a slope of $1/2$.

It is worth noting that models 1 and 2 must have the RRW noise included in the simulation of the gyroscope signal, otherwise the measurement of the bias instability by the Allan deviation provides an incorrect value due to possible incorrect measurement of the minimum point. The Allan deviation without RRW does not have the characteristic increase at the end, therefore the minimum value can be used incorrectly to calculate the bias instability.

After validating the simulated signals by comparing the recovered noise values by using the Allan variance method, model 3, built in Simulink, was included inside the navigation and control algorithm of the satellite launch vehicle of [1] (Sensors block in Fig. 1). Model 3 was chosen for simplicity because the vehicle simulation was also created in Simulink. One gyroscope model was used for each rotation axis, representing the angular velocity measurements $\dot{\phi}$, $\dot{\theta}$, and $\dot{\psi}$. Where ϕ (roll), θ (pitch), and ψ (yaw) are the Euler angles.

Simulations were carried out exactly as explained in [1], using the simulation diagram as in Fig. 1. For more details of the desired trajectory and planned maneuver for the vehicle refer to this cited reference. First, a simulation considered an ideal gyroscope without noises, where the angular velocities recovered are exactly the vehicle angular velocities. Then, a simulation considered the IFOG model with noises representing the IFOG from [8], maintaining all other sensors as ideal sensors in the simulation.

Finally, with the results from the control and navigation algorithm considering ideal gyroscopes and IFOGs, the vehicle trajectory can be drawn to assess the viability of using an IFOG made with Brazilian technology for this navigation application.

IV. RESULTS

Models 1, 2, and 3 were simulated with the same input values for the noises and the same bandwidth. Each simulation generated an output signal with 3.6 million points for each model. The output of the simulations can be seen in Fig. 6.

Taking the time domain signals generated by the models (Fig. 6) and performing the Allan variance calculation, the Allan deviation is plotted for the three results, as shown in Fig. 7 (together with the Allan deviation of the MEMS gyroscope used as comparison which was simulated using model 3).

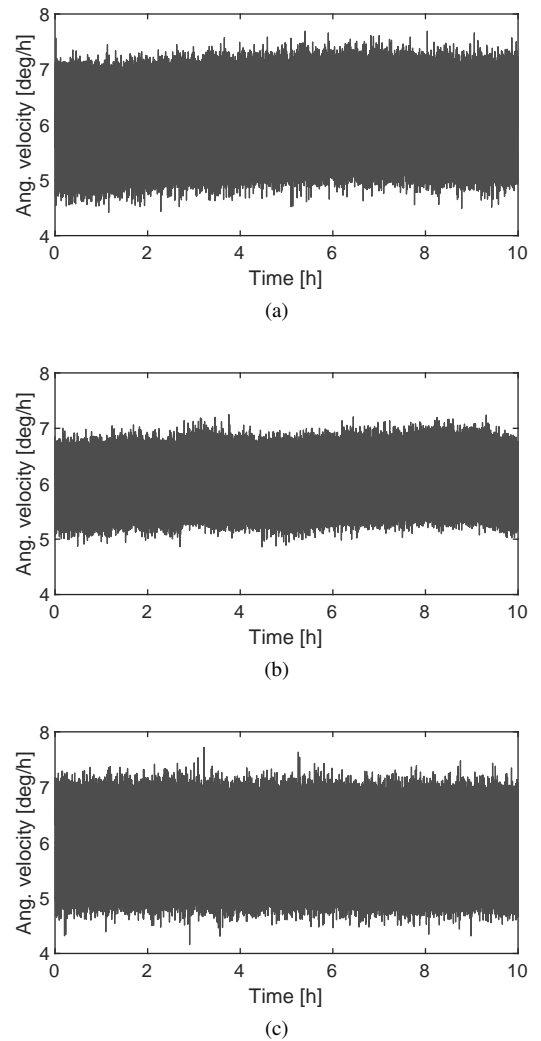


Fig. 6. Results of IFOG simulations using (a) model 1, (b) model 2, and (c) model 3.

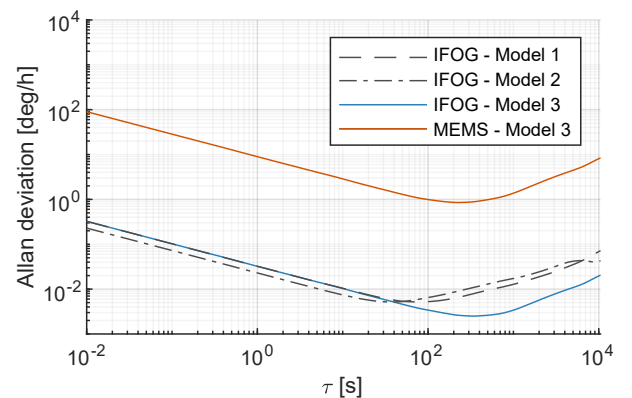


Fig. 7. Allan deviation of the three gyroscope models.

By performing a visual analysis in the Allan deviation log-log scale plot (Fig. 7), the noise values could be recovered and are presented in Table I. The recovered noise values of ARW, bias instability, and RRW are all in the same order of magnitude among the three models. Also, they are in the same order of magnitude as the input reference values for the noises (first line of Table I). The reference values of ARW and bias instability were measured experimentally by [8].

To provide a quantitative perspective of the noise values

TABLE I
VALUES RECOVERED FROM SIMULATIONS

	ARW [$^{\circ}/\sqrt{h}$]	Bias instability [$^{\circ}/h$]	RRW [$^{\circ}/h/\sqrt{h}$]
Reference values	$\dagger 5.40 \cdot 10^{-4}$	$\dagger 1.70 \cdot 10^{-3}$	$4.32 \cdot 10^{-2}$
Model 1	$5.40 \cdot 10^{-4}$	$8.11 \cdot 10^{-3}$	$4.51 \cdot 10^{-2}$
Model 2	$3.81 \cdot 10^{-4}$	$7.93 \cdot 10^{-3}$	$5.86 \cdot 10^{-2}$
Model 3	$5.40 \cdot 10^{-4}$	$3.77 \cdot 10^{-3}$	$1.10 \cdot 10^{-2}$
MEMS - Reference	$\ddagger 0.15$	$\ddagger 0.70$	4.32
MEMS - Model 3	0.15	1.28	4.32

\dagger Values from [8]. \ddagger Values from [14].

recovered, the IFOG values from Table I were converted to Table II, where only the IFOG values were used to validate the models. The error percentage in relation to the reference values that were used as input was calculated by

$$\text{Error} = \frac{\text{Recovered value} - \text{Reference value}}{\text{Reference value}} \times 100\%. \quad (3)$$

The results in Table II showed a great discrepancy in the bias instability recovered values. However, this discrepancy among the bias instability errors in percentage might not be read as a failure, because the worst magnitude difference is only $6.41 \cdot 10^{-3}$. In [15], although the error for the simulated bias instability is only 7.58 %, the error absolute value is $1.7 \cdot 10^{-3}$ which is within the same order of magnitude as in this work. Considering the simulation uses pseudo-random numbers and each simulation can provide slightly different results, for being in the same order of absolute error, all three simulations can be considered a valid model to represent the chosen IFOG.

TABLE II
ERROR BETWEEN IFOG REFERENCE VALUES USED AS INPUT AND IFOG RECOVERED NOISES

	ARW	Bias instability	RRW
Model 1	0.05 %	376.99 %	4.37 %
Model 2	-29.46 %	366.44 %	35.74 %
Model 3	-0.02 %	121.70 %	-74.49 %

Then, IFOG simulated using model 3 and the MEMS gyroscope simulated with model 3 were inserted in the control and navigation algorithm from Fig. 1. The recovered trajectory of the rocket is shown in three dimensions in Fig. 8, showing a trajectory in only 2 directions.

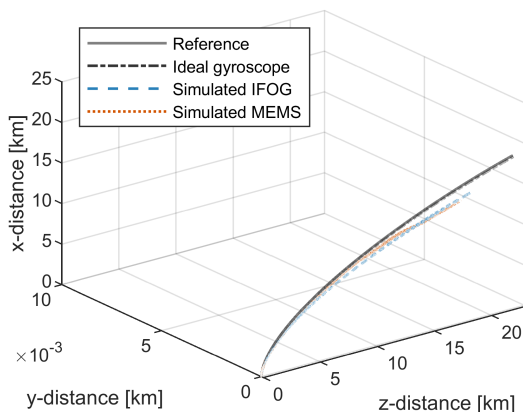


Fig. 8. Comparison among the simulated trajectories.

Then, for better visualization, the plot can be seen in two dimensions in Fig. 9. The difference between the reference trajectory and the trajectory calculated using an ideal gyroscope is 0.20 km ($\approx 1\%$ error). The difference between the reference trajectory and the trajectory with the IFOG is 4.66 km ($\approx 16\%$ error). The difference between the reference trajectory and the trajectory with the MEMS is 5.92 km ($\approx 20\%$ error). The inset in Fig. 9 shows a difference of approximately 1 km in each direction between the simulated trajectory using the IFOG and the MEMS gyroscope, being the trajectory using the IFOG the nearest to the reference trajectory.

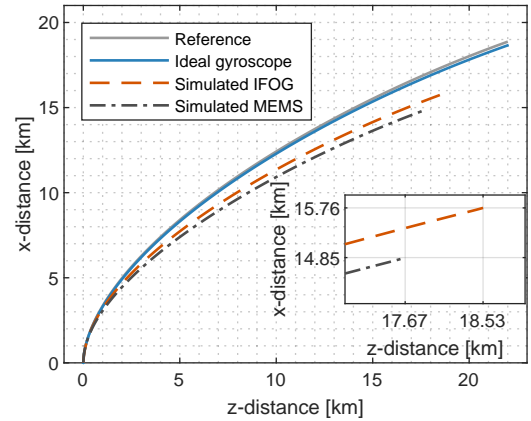


Fig. 9. Comparison among the simulated trajectories.

The trajectory controller implemented in this MLV simulation comprises only the attitude control of the vehicle, so it is more representative to analyze the attitude than the final trajectory. Fig. 10 shows the reference attitude over time compared to the attitude measured using the IFOG and the MEMS gyroscope. In Fig. 10a, one can see the pitch stability provided by the control implemented by [1] with both gyroscopes. In its inset, it is possible to notice the greater noise in the angle measurement by the MEMS when compared to the IFOG, however, it is not enough to make the feedback loop unstable. Fig. 10b shows the yaw stability compared to the reference. Both sensors provide an error of less than 0.4° similar amplitudes between them, but with the IFOG error starting later than the MEMS gyroscope error.

V. CONCLUSION

Three models to simulate characteristics of a real IFOG were presented and explained in this work. All models were validated by characterization of the output signals using the Allan variance method. An IFOG simulation built in Simulink (model 3), representing an IFOG made in Brazil, was implemented together with the navigation and control algorithm of a microsatellite launch vehicle. Then, it was compared with a simulation using a MEMS gyroscope and the same control algorithm.

The results showed that the navigation and control algorithm used was able to correctly stabilize the vehicle's attitude. However, it still requires improvements in order to follow the desired trajectory.

For future works, it is intended to implement more elements in the navigation and control algorithm to follow a reference trajectory. Also, it is intended to simulate a longer vehicle

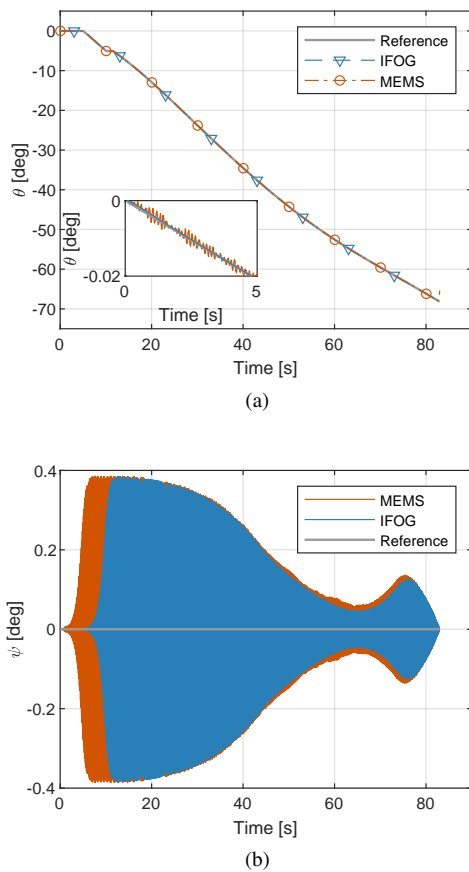


Fig. 10. Attitude over time.

travel to analyze the effects of the IFOG noises when working during a longer time.

VI. ACKNOWLEDGMENTS

This work was financed in part by FINEP under the agreement 01.20.0207.00 and by FAPEMA.

REFERENCES

- [1] A. J. A. Tavares Júnior, "Desenvolvimento e simulação de um computador de bordo para o veículo lançador de microssatélites (VLM)," Master's thesis, Universidade Estadual do Maranhão, São Luís, 2019. [Online]. Available: <http://repositorio.uema.br/jspui/handle/123456789/1252>
- [2] A. C. Boley and M. Byers, "Satellite mega-constellations create risks in low earth orbit, the atmosphere and on earth," *Scientific Reports*, vol. 11, no. 1, pp. 1–8, 2021. [Online]. Available: <https://doi.org/10.1038/s41598-021-89909-7>
- [3] E. O. Doebelin, *Measurement systems application and design*, 5th ed. McGraw-Hill, 2007.
- [4] H. G. Wang and T. C. Williams, "Strategic inertial navigation systems - high-accuracy inertially stabilized platforms for hostile environments," *IEEE Control Systems Magazine*, vol. 28, no. 1, pp. 65–85, 2008. [Online]. Available: <https://doi.org/10.1109/MCS.2007.910206>
- [5] L. Wang, W. Wang, Q. Zhang, and P. Gao, "Self-calibration method based on navigation in high-precision inertial navigation system with fiber optic gyro," *Optical Engineering*, vol. 53, no. 6, p. 064103, 2014.
- [6] S. L. Sabat, N. Giribabu, J. Nayak, and K. Krishnaprasad, "Characterization of fiber optics gyro and noise compensation using discrete wavelet transform," in *2009 Second International Conference on Emerging Trends in Engineering & Technology*. IEEE, 2009, pp. 909–913. [Online]. Available: <https://doi.org/10.1109/ICETET.2009.50>
- [7] E. Udd, "An overview of the development of fiber gyros," in *Optical Waveguide and Laser Sensors*, R. A. Lieberman, G. A. Sanders, and I. U. Scheel, Eds., vol. 11405, International Society for Optics and Photonics. SPIE, 2020, p. 1140502. [Online]. Available: <https://doi.org/10.1117/12.2557455>

- [8] R. M. Bacurau, A. Dante, M. W. Schlichting, A. W. Spengler, and E. C. Ferreira, "Two-level and two-period modulation for closed-loop interferometric fiber optic gyroscopes," *Opt. Lett.*, vol. 43, no. 11, pp. 2652–2655, Jun 2018. [Online]. Available: <https://www.doi.org/10.1364/OL.43.002652>
- [9] A. G. Silva, "Análise e projeto de sistemas de controle de atitude para o veículo lançador de satélites (VLS)," Master's thesis, Instituto Nacional de Pesquisas Espaciais (INPE), São José dos Campos, 2014-02-26 2014. [Online]. Available: <http://urlib.net/ibi/8JMKD3MGP5W34M/3FSB348>
- [10] G. da Silveira, "Desenvolvimento de uma ferramenta computacional para simulação de voo de veículos lançadores," Master's thesis, Instituto Nacional de Pesquisas Espaciais (INPE), São José dos Campos, 2014.
- [11] D. Titterton and J. L. Weston, *Strapdown inertial navigation technology*, 2nd ed. IET, 2004.
- [12] H. C. Lefèvre, *The fiber-optic gyroscope*. Artech house, 2014.
- [13] W. Stockwell, *Angle random walk*, Crossbow Technology, Inc, 2003.
- [14] B. Braun, J. Barf, and M. Markgraf, "Integrated navigation using MEMS-based inertial, GPS and sun vector measurements aboard the spin-stabilized PMWE-1 sounding rocket," in *8th European Conference for Aeronautics and Space Sciences (EUCASS), EUCASS2019-241*, 2019. [Online]. Available: <https://doi.org/10.13009/EUCASS2019-241>
- [15] K. Jerath, S. Brennan, and C. Lagoa, "Bridging the gap between sensor noise modeling and sensor characterization," *Measurement*, vol. 116, pp. 350–366, 2018. [Online]. Available: <https://doi.org/10.1016/j.measurement.2017.09.012>
- [16] Y. Paturel, *How to select the right IMU?*, iXblue, 2020. [Online]. Available: <https://www.ixblue.com/resource/ixlive/how-to-select-the-right-imu/>
- [17] J. M. Wheeler, J. N. Chamoun, V. Dangui, and M. J. F. Dignonnet, "Analytic method for estimating aircraft fix displacement from gyroscope's allan-deviation parameters," *IEEE Sensors Journal*, vol. 22, no. 5, pp. 4207–4214, 2022. [Online]. Available: <https://doi.org/10.1109/JSEN.2022.3145012>
- [18] M. S. Bielas, "Stochastic and dynamic modeling of fiber gyros," in *Fiber Optic and Laser Sensors XII*, R. P. DePaula, Ed., vol. 2292, International Society for Optics and Photonics. SPIE, 1994, pp. 240 – 254. [Online]. Available: <https://doi.org/10.1117/12.191837>
- [19] M. M. Carvalho and R. M. Cazo, "Noise analysis in a fiber bragg grating accelerometer using allan variance method," in *Third Asia Pacific Optical Sensors Conference*, J. Canning and G. Peng, Eds., vol. 8351, International Society for Optics and Photonics. SPIE, 2012, pp. 272 – 277. [Online]. Available: <https://doi.org/10.1117/12.915804>
- [20] J. Li and J. Fang, "Not fully overlapping allan variance and total variance for inertial sensor stochastic error analysis," *IEEE Transactions on Instrumentation and Measurement*, vol. 62, no. 10, pp. 2659–2672, 2013. [Online]. Available: <https://doi.org/10.1109/TIM.2013.2258769>
- [21] S. M. Yadav, S. K. Shastri, G. B. Chakravarthi, V. Kumar, and D. R. A., "A fast, parallel algorithm for fully overlapped allan variance and total variance for analysis and modeling of noise in inertial sensors," *IEEE Sensors Letters*, vol. 2, no. 2, pp. 1–4, 2018. [Online]. Available: <https://doi.org/10.1109/LSENS.2018.2829799>
- [22] S. P. Maddipatla, H. Haeri, K. Jerath, and S. Brennan, "Fast allan variance (FAVAR) and dynamic fast allan variance (D-FAVAR) algorithms for both regularly and irregularly sampled data," *IFAC-PapersOnLine*, vol. 54, no. 20, pp. 26–31, 2021, modeling, Estimation and Control Conference MECC 2021. [Online]. Available: <https://doi.org/10.1016/j.ifacol.2021.11.148>
- [23] *IEEE Standard for Specifying and Testing Single-Axis Interferometric Fiber Optic Gyros*, 2021, IEEE Std 952-2020. [Online]. Available: <https://doi.org/10.1109/IEEESTD.2021.9353434>